ACS APPLIED MATERIALS & INTERFACES

Research Article

www.acsami.org

Investigation of Interfacial Adhesion between the Top Ends of Carbon Nanotubes

Jungwook Choi, Youngkee Eun, and Jongbaeg Kim*

School of Mechanical Engineering, Yonsei University, 50 Yonsei-ro, Seodaemun-gu, Seoul 120-749, Republic of Korea

Supporting Information

ABSTRACT: Understanding the interfacial forces of carbon nanotubes (CNTs) is fundamental to the development of electromechanical systems based on the contact of CNTs. However, experimental studies on the adhesion properties between CNTs are scarce despite the remarkable contact quality of CNTs. Here, we present an experimental investigation of the adhesion between the top ends of aligned, self-adjusted CNTs using a CNT-integrated microelectromechanical actuator. The pull-out and pull-in behaviors of the contact as a function of the applied force by the actuator are precisely identified by measuring the contact resistance between the CNTs. The adhesion between the top ends of individual CNTs is extracted from the measured adhesive strength between the CNT arrays, and it agrees with the theoretical values of the van der Waals interactions. By exploiting the adhesion of the CNT-to-CNT contact, a programmable and reliable microelectromechanical switching device is demonstrated. Our results offer design strategies for diverse CNT-based nano- and microelectromechanical devices that need repeatable contacting interfaces.

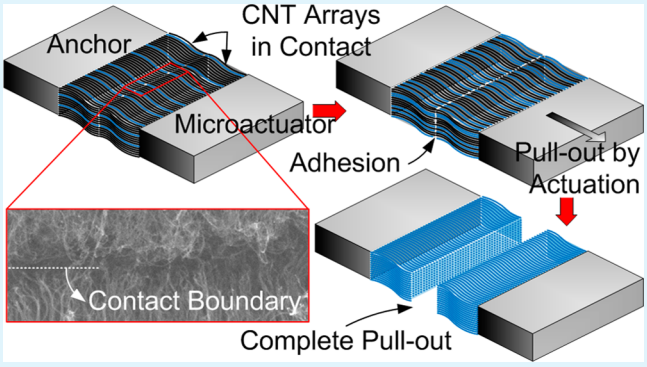

KEYWORDS: *carbon nanotube, self-adjusted carbon nanotube array, adhesion, adhesive strength, van der Waals force, electromechanical switch*

INTRODUCTION

The interfacial forces of one-dimensional nanostructures have been explored for use as artificial adhesives.[1,2] Among them, carbon nanotubes (CNTs) are promising candidates for diverse applications of dry adhesives, and their adhesive characteristics have attracted great attention.[3−9] For example, vertically aligned CNT arrays showed remarkable macroscopic adhesive strengths up to 29 and 100 N cm^{-2} in the normal[5] and shear[8] directions, respectively. These adhesive strengths are due to the high mechanical strength, high resilience, high aspect ratio, and high areal number density of CNTs, leading to strong van der Waals forces between the target surfaces.[1,5] In addition to the macroscopic adhesive properties of aligned CNT arrays, the work of adhesion between an individual multiwalled CNT and a glass surface was estimated to be around 300 mJ m^{-2},[10] and the corresponding adhesive strength was predicted to be over 500 N cm^{-2} based on the Johnson−Kendall−Roberts theory of elastic contact.[4,11] Studies using atomic force microscopy (AFM) also reported that the adhesion between the sidewall of a single-walled CNT and the hydroxyl-functionalized AFM probe exhibited 8.7 ± 6.7 nN of adhesion force.[12] Furthermore, when AFM was used to apply a vertical load on a suspended CNT, an axial tension of 7−8 nN in the single-walled CNT was required to cause slip across a silicon dioxide surface.[13]

Although several works reported the interfacial forces between CNTs and other solid surfaces, only a few experimental works have studied the adhesion forces between CNTs.[14−17] However, direct CNT-to-CNT contact has been adopted in diverse applications such as nanotweezers,[18] nanoelectromechanical switches,[19−21] micromechanical contact materials,[22,23] and dry adhesives in high-temperature silicon (Si) processing.[24] These CNT-based contacts offer distinctive functionalities over conventional solid-to-solid contacts such as suppressing noise and increasing the durability of sliding electrical contacts,[25,26] improving contact reliability and high current density transmission capability,[22] and extending inertial switch contact times.[23] Because adhesion plays an important role in determining the performance and reliability of the CNT-based devices, a quantitative experimental investigation on the interfacial forces between CNTs is imperative and may offer guidelines for potential CNT-to-CNT contact-based applications.

In this work, we measured and characterized the adhesion between the top ends of aligned CNTs for the first time using a CNT-integrated electrostatic microelectromechanical actuator. The CNTs are grown inside a gap between the actuator and the facing fixed electrode, making contact at their top ends. The actuator is devised to be bidirectionally movable in the

Received: January 13, 2014
Accepted: March 31, 2014
Published: March 31, 2014

   dx.doi.org/10.1021/am500252s | ACS Appl. Mater. Interfaces 2014, 6, 6598−6605

direction parallel to the CNT alignment. Hence, the actuator provides a well-controlled contact force and pull-out force in the sub-μN range as well as high-frequency operation over a few hundred hertz for facile, multiple, and repeatable measurements in diverse environments. The on-state, where the CNTs are in contact, and off-state, where the CNTs are apart, are controlled by the actuation force applied and monitored in real time by a current flowing through the contact with high resolution and accuracy. It is found that the van der Waals force is primarily responsible for the adhesion between the CNTs, and the estimated adhesion between the top ends of individual CNTs is 0.133 ± 0.109 nN in ambient conditions. Compared to previously reported adhesions between crossed or parallel sidewalls of CNTs in the range of 0.126–6 nN,[14−17] our lower bound result is smaller possibly because of the small contact area between the top ends of the CNTs. Moreover, the adhesive strength between CNT arrays in the normal direction is 0.054 N cm^{-2} at a contact force of 0.058 N cm^{-2}, which is 10^2–10^3 times lower than the macroscopic adhesion of CNT arrays on a glass surface.[3−9] Nevertheless, this low adhesive strength is sufficient to maintain the relative position of movable structures in microscale devices. Accordingly, we successfully demonstrate a programmable microelectromechanical switch with write, erase, and read functionality using the adhesion properties of CNT-to-CNT contact.

RESULTS AND DISCUSSION

Two sets of CNT arrays were integrated on a bidirectional and electrostatic actuator, which is composed of a source electrode, a shuttle connected to a drain electrode by a spring, and two comb-shaped gate electrodes, as illustrated in Figure 1a. Applying a voltage on each gate electrode (V_{G1} and V_{G2}) enabled the bidirectional actuation of the shuttle, while the current flowing from the source to the drain electrode through the contact between the CNT arrays (I_{SD}) was monitored. Because of the length distribution of the CNTs, longer CNTs inside the arrays grown on the anchor (source) electrode were initially in contact with those grown on the shuttle (drain) electrode at their top ends, whereas the shorter CNTs remained disconnected (Figure 1b). Upon application of V_{G1} and the corresponding electrostatic force on the shuttle, the contact between the top ends of the CNTs began to gradually separate from the shorter CNTs against the adhesion between them (Figure 1c). On the other hand, the shuttle was driven toward the source electrode when V_{G2} was applied, and this actuation increased the total contact force between the CNTs (Figure 1d). The larger contact force increased the number of CNTs in contact, leading to an increase in the adhesive strength (adhesion per unit area) and a decrease of the contact resistance (increased I_{SD} at identical V_{SD}) between the CNT arrays. When V_{G1} exceeded the pull-out voltage, the CNTs were completely separated, and the contact resistance between the CNTs became infinity (Figure 1e).

The microstructures were batch-fabricated by bulk micromachining on a Si-on-insulator wafer with a 20-μm-thick heavily doped Si device layer. Then a 5-nm-thick iron catalyst was selectively deposited on the sidewalls of the anchor and the shuttle, and the CNT arrays were grown by chemical vapor deposition (CVD; Figure S1 in the Supporting Information, SI). The CNT arrays were self-adjusted during the CVD, forming the contact boundary in the middle of the gap between the anchor and the shuttle.[27] The scanning electron microscopy

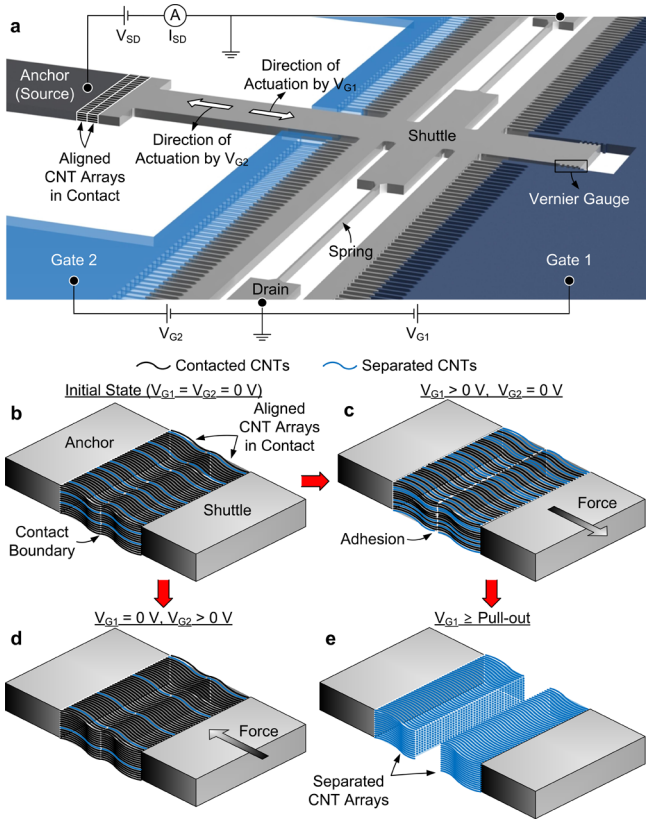

Figure 1. (a) Schematic of the bidirectional electrostatic actuator with integrated CNT arrays and the electrical circuit configuration used for adhesion measurement. Applying voltage on gate 1 (V_{G1}) allows pull-out of the contact, whereas the total contact force increases by increasing the voltage on gate 2 (V_{G2}). To verify the status of the contact, the current (I_{SD}) between the source and the drain is monitored during actuation. (b) CNTs initially make contact at their top ends, while some of the shorter CNTs are discontiguous. (c) The number of CNTs in contact is gradually decreased as the applied V_{G1} and electrostatic force increase. (d) Increasing V_{G2} increases the number of CNTs in contact (i.e., real area of contact). (e) The contact is separated only when the electrostatic force by V_{G1} exceeds the sum of the contact force and adhesion.

(SEM; Hitachi S-4300) image in Figure 2a shows the CNT-integrated bidirectional actuator. The top view of the two sets of CNTs and their contact boundary is shown in Figure 2b. When the two facing CNT arrays were in contact, the CNT arrays did not penetrate into each other even under an increased compressive load[28] because of the van der Waals interactions and the high areal number density. Therefore, the extrusive growth force[29] of the self-adjusted CNTs strained the spring of the actuator. Hence, the aligned CNT arrays were grown under a compressive load by the restoring force of the deformed spring, and at the same time, the contact was preloaded. As a result, the CNTs had tortuous morphology, as shown in Figure S2a in the SI. Moreover, the CNT arrays made contact at the ends without mechanical interlocking at the sidewalls, as shown in Figure 2b. The contact geometries between the CNTs would be point contacts such as sphere–sphere and crossed cylinder–cylinder, as illustrated in the inset of Figure 2b. To clearly observe the top ends of the CNTs, the counter CNT array was intentionally removed, as shown in Figure 2c, and it consisted of both straight and curled tips of the CNTs. Using transmission electron microscopy (TEM;

dx.doi.org/10.1021/am500252s | ACS Appl. Mater. Interfaces 2014, 6, 6598–6605

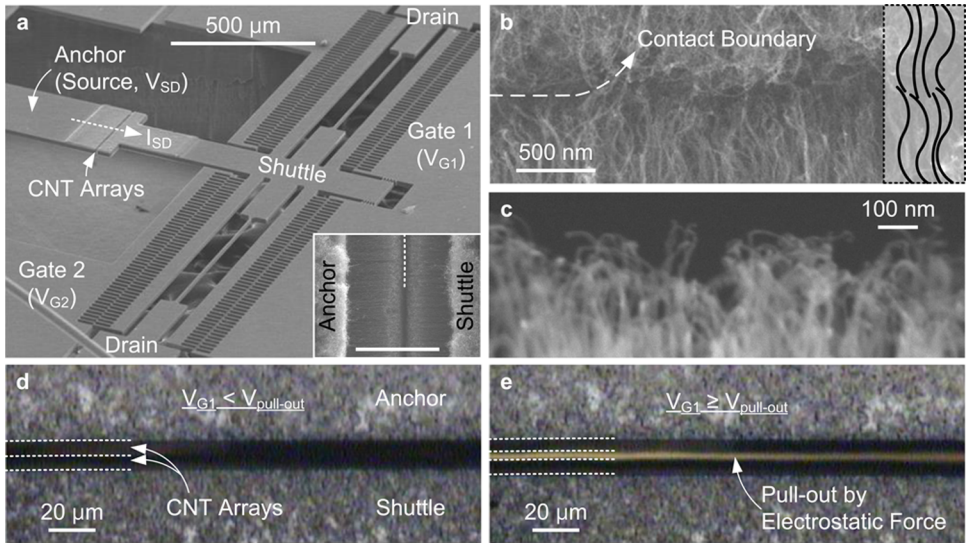

Figure 2. (a) SEM image of the CNT-integrated bidirectional actuator with source, shuttle (drain), and two gate electrodes. The inset shows the top-view SEM image of the aligned CNT arrays in contact. The length of each CNT array is 6.5 μm, and they make contact in the middle of the gap between the anchor (source) and the shuttle. The scale bar is 10 μm. (b) The enlarged contact region between the CNT arrays shows that only the top ends contact and the CNTs are not interlocking. The inset shows possible contact geometries between the top ends of the CNTs. (c) The top ends of the CNTs have both straight and curled tips. (d and e) Optical microscopy images of the contact according to the applied V_{G1}. The on-state where the CNTs are in contact is maintained by the adhesion until V_{G1} reaches the pull-out voltage (43.5 V).

JEOL JEM-4010), we observed that the CNTs had a multiwalled structure with an average external diameter of 10 nm (Figure S2b in the SI). The micro-Raman spectroscopy (Jobin Yvon LabRam HR, 514 nm argon-ion laser with 0.5 mW output power and 1 μm spot diameter) also confirmed the multiwalled structure of the CNTs with D and G peaks at 1350 and 1585 cm^{-1}, respectively (Figure S2c in the SI).

The optical microscopy images in Figure 2d,e show the contact between the CNTs with respect to an applied V_{G1}. The CNT arrays were initially in contact (low electrical resistance, on-state) until V_{G1} reached the pull-out voltage. The contact was separated at the pull-out voltage (high electrical resistance, off-state) by a 2 μm air gap when the shuttle was electrostatically actuated. We can easily measure the displacement of the shuttle ($d_{shuttle}$) with a Vernier gauge, which was devised as a part of the actuator (Figure S3a in the SI). After CNT growth, the shuttle displacement was 3 μm (Figure S3b in the SI). Without applying bias at the gates, the corresponding initial contact force was estimated to be 3.45 μN based on the measured stiffness of the spring (k_{spring}) of 1.15 N m^{-1} (Figure S4 in the SI). During the shuttle actuation by V_{G1} of 43.5 V, the shuttle displacement was 5 μm (Figure S3c in the SI), and the contact between the CNTs was disengaged.

To characterize the adhesive strength between the CNT arrays, the pull-out and pull-in behaviors were monitored by measuring the current (I_{SD}) between the source and drain electrodes under a constant bias voltage (V_{SD}) of 1 V, while V_{G1} was swept between 0 and 55 V. As shown in Figure 3a, the I_{SD}–V_{G1} characteristics exhibited hysteretic behavior because of adhesion between the CNTs. In the forward sweep, I_{SD} was gradually decreased, implying that the number of CNTs in contact decreased. During this pull-out process, the buckled and curled CNTs could be straightened and elongated owing to the adhesion between them, and the shorter CNTs inside the array would separate earlier than the longer ones. At V_{G1} = 43.5 V, the two sets of CNTs were completely separated (pull-out), and accordingly, I_{SD} was not delivered through the contact. On the other hand, in the reverse sweep, a portion of CNTs made contact at 40 V (pull-in), and I_{SD} started to flow through the contact again. Unlike solid-to-solid contacts, which have sudden and sharp pull-in behavior, the contact between the CNT arrays exhibited gradual pull-in behavior. Because the lengths of the CNTs inside the arrays are distributed and each CNT acts as an elastic contact site, the number of CNTs in contact increases as the shuttle moves toward the source electrode after pull-in. As a result, I_{SD} increased until V_{G1} reached 9.5 V in the reverse sweep, where it became identical with the initial state.

The contact can be disengaged only when the electrostatic force by V_{G1} overcomes the adhesion and contact force (see the SI for a detailed force balance during pull-out). Because the contact is preloaded by the restoring force of the spring, which is strained by the extrusive growth force of the CNTs after the growth process is terminated, the amount of the initial contact force is equal to the restoring force of the spring. Thus, the adhesion (F_{Adh}) between the top ends of the CNT arrays is numerically defined as the difference between the electrostatic force ($F_{P.O.}$) at the pull-out voltage ($V_{P.O.}$) and the contact force ($F_{Contact}$) by the strained spring

$$F_{Adh} = F_{P.O.} - F_{Contact} = \frac{\varepsilon t_{comb} n_{comb} V_{P.O.}^{2}}{2g} - k_{spring} d_{shuttle}$$

where ε, t_{comb}, n_{comb}, and g represent the free space permittivity, the height of the comb finger, the number of comb pairs, and the gap between comb fingers, respectively. Alternatively, the electrostatic force can be more precisely estimated by the finite element method (Figure S5 in theSI). The average adhesion between the CNT arrays in the normal direction was 3.24 μN (0.054 N cm^{-2}) at a contact force of 3.45 μN (0.058 N cm^{-2}). The macroscopic contact made by high contact force around tens of N cm^{-2} applied between CNT arrays and flat surfaces formed a line contact by the sidewall of entangled CNT segments, and therefore the resultant high adhesive strength of 100 N cm^{-2} was achieved.[8] However, the point contact

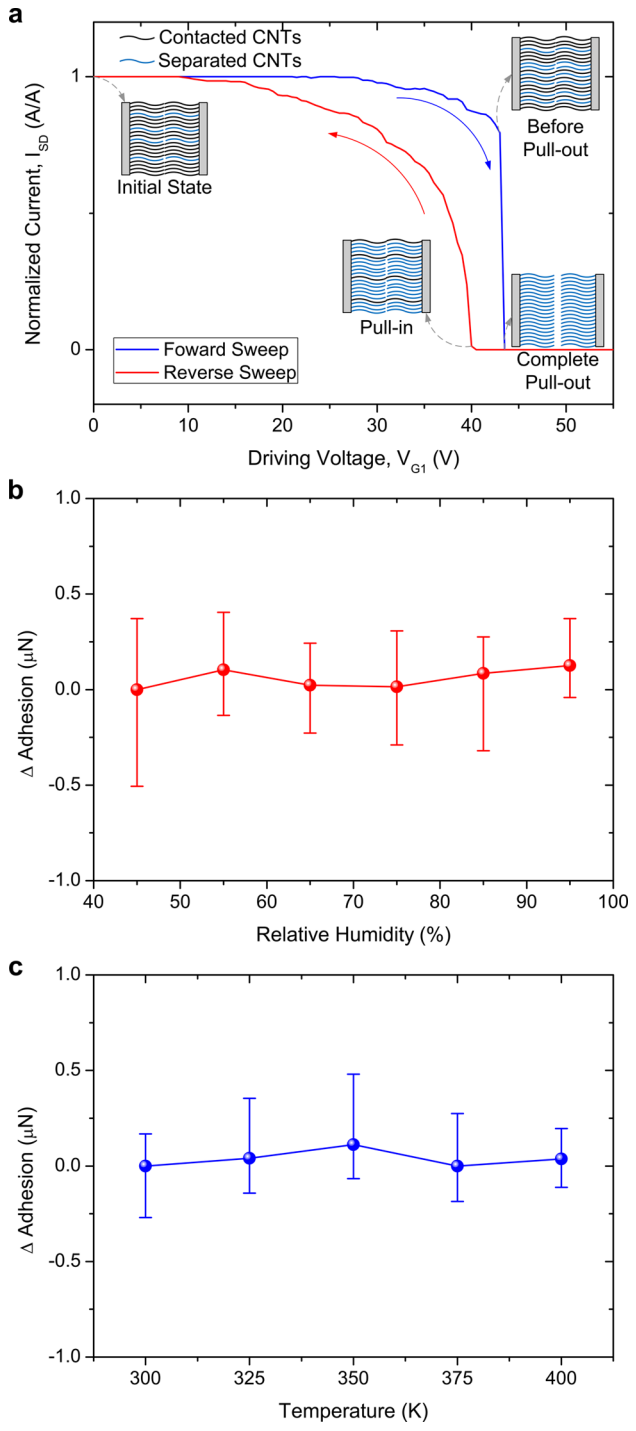

Figure 3. (a) The $I_{SD}-V_{G1}$ curve shows the hysteretic behavior due to adhesion between the CNTs. The pull-out and pull-in voltages are 43.5 and 40 V, respectively. (b) The adhesion is independent of the RH, indicating a negligible capillary force effect. (c) Owing to the high thermal stability of the contact between the CNTs, softening and welding, which would lead to high adhesion, are not observed as the temperature is increased.

between the top ends of CNTs without mechanical sidewall interlocking results in low adhesion. The adhesive strength in this work was obtained from the apparent contact area of 300 × 20 μm^2 where the CNT arrays were grown and came in contact. Increasing the number density of the CNTs would further increase the adhesive strength.

The total adhesion between the CNT arrays would be the sum of the adhesion between individual CNTs. The number of CNTs in contact can be estimated by measuring the resistance between the source and the shuttle just before pull-out. The resistance here includes the CNT/Si junctions, the CNT arrays, and the CNT/CNT contacts connected in series. On the basis of the contact resistivity between the CNTs and heavily-doped Si (10^{-5}–10^{-4} Ω cm^2),[30,31] the resistivity of aligned, multi-walled CNT arrays (0.25 × 10^{-4}–1 × 10^{-4} Ω m),[32] the junction resistance between the CNTs (98–2677 kΩ),[33] and the measured average resistance between the source and the shuttle of 1.902 kΩ, the areal number density of CNTs in contact could be in the range of 2.24 × 10^8–2.26 × 10^9 cm^{-2} (see the SI for the detailed estimation process). It is noted that the resistance of the CNT/Si junction dominates the entire resistance, and it is less dependent on the growth conditions. Compared with the previously reported typical number density of aligned CNTs (~10^9–10^{10} cm^{-2}),[29,34] in our case, a lower number of CNTs made contact with their top ends. Therefore, by dividing the adhesion between the CNT arrays by the number of CNTs in contact, the adhesion between the top ends of two CNTs, which have an average diameter of 10 nm, is estimated to be 0.133 ± 0.109 nN. The diameter of the CNTs, their contact geometries, the environmental conditions for measurements, and the corresponding adhesions between two CNTs are compared to previous experimental works and are summarized in Table S1 in the SI.

The interfacial attractive forces generally originate from a combination of the van der Waals forces, the capillary forces, the electrostatic forces, and the softening and welding between asperities of two solids in contact.[35] The friction between CNTs is not considered here because the CNTs are pulled out in the normal direction without experiencing sliding. To elucidate the mechanism and verify the effect of the capillary forces on the adhesion between CNTs, we measured the dependence of adhesion on the relative humidity (RH) from 45 to 95% under atmospheric pressure at a constant temperature of 298 K. As shown in Figure 3b, the relative changes of adhesion were independent of the RH level, which revealed negligible capillary force effects. At higher RH, additional water molecules could condense between asperities of the contact surfaces, and the Laplace pressure across the meniscus contributes to an increase of the adhesion. However, the hydrophobicity of the aligned CNTs[36] suppresses the condensation of water molecules and minimizes the capillary force acting on the contact interface. Furthermore, a higher temperature accelerates the softening of surfaces, leading to strong adhesion in typical metal-to-metal contacts.[35] However, as shown in Figure 3c, the adhesion between CNTs does not depend on the temperature when the temperature is increased from 300 to 400 K. On the investigation of the adhesion under different environmental conditions, the dependence of the relative permittivity of air on the RH and temperature was considered because it could be related to calculation of the pull-out electrostatic forces. In the above RH and temperature ranges, however, the relative permittivity of air had little dependence on the RH and temperature;[37] thus, the corresponding change in electrostatic forces due to environmental differences would be negligible. This minimal capillary effect and high thermal stability of the CNT-to-CNT contact would be advantageous for improving the reliability of electromechanical switches and relays in humid, high-temperature environments.

dx.doi.org/10.1021/am500252s | ACS Appl. Mater. Interfaces 2014, 6, 6598–6605

Because of the high conductivity of both the Si structures and the CNTs, the electrostatic charging-induced forces may not significantly contribute to the adhesion. Therefore, we may conclude that the van der Waals forces are the major cause of the adhesion between the top ends of the CNTs. Considering the possible contact geometries between the CNTs described in the inset of Figure 2b, the van der Waals forces (F_{vdw}) can be expressed as[38] $F_{vdw} = Ar/12D^2$ for tip-to-tip contact of the CNTs and $F_{vdw} = Ar/6D^2$ for contact between the crossed sidewalls of the CNTs. Here, A is the Hamaker constant between the CNTs (2.842×10^{-20} J),[39] r is the radius of the CNT (5 nm), and D is the distance between the CNTs that maximizes the attractive force (0.34 nm).[8] In these cases, the van der Waals forces are 0.102 and 0.205 nN, respectively, and this agrees well with our estimation of 0.133 ± 0.109 nN. It also suggests that the contact geometries between the CNTs in our experiments are a combination of the sphere−sphere and crossed cylinder−cylinder geometries. Compared to previous reports on the shear-sliding behavior and the van der Waals interaction between nested walls in multiwalled CNT,[40,41] the van der Waals force between the top-end contact of CNTs is a few orders of magnitude lower than that of the nested wall because of the different contact geometries that strongly influence the resultant van der Waals forces.

The current−voltage (I_{SD}−V_{SD}) characteristics of the contacts were measured according to the voltage applied on gate 2 (V_{G2}), as shown in Figure 4a. When V_{G2} was increased from 0 to 25 V, the total contact force between the CNTs increased. As a result, both the number of CNTs in contact and the contact area between the CNTs would increase upon the elastic bending of the CNTs, and accordingly the contact resistance decreased. It is noted that the change in resistance would dominantly result from the contact resistance between the CNTs rather than the coupling of the CNTs within the arrays.[42] I_{SD} under a constant V_{SD} of 3 V and the total contact force controlled by V_{G2} are well matched (Figure 4b), implying that the real area of contact between the two sets of CNT arrays increases as the contact force increases. Thus, it is expected that the adhesion between the CNT arrays would increase as a function of the contact force. The adhesion dependence on the contact force was also investigated by applying a voltage on V_{G2}, while recording the I_{SD}−V_{G1} hysteresis. The average pull-out voltages on V_{G1} were increased to 44.9, 48.4, and 53.8 V at V_{G2} of 10, 20, and 30 V, respectively (Figure S6 in the SI). Consequently, the adhesion between the CNT arrays increased from 3.24 μN (0.054 N cm^{-2}) to 3.59 μN (0.060 N cm^{-2}) when the contact force was increased from 3.45 μN (0.058 N cm^{-2}) to 6.64 μN (0.111 N cm^{-2}), as shown in Figure 4c. The adhesion between individual CNTs is not significantly dependent on the contact forces. The average resistance between the source and the shuttle before pull-out was 1.889, 1.847, and 1.758 kΩ at V_{G2} of 10, 20, and 30 V, respectively. Using these values with the methods previously discussed, we could obtain the number of CNTs in contact with respect to the contact force, and the adhesion between individual CNTs was 0.134 ± 0.110, 0.135 ± 0.111, and 0.136 ± 0.111 nN in each case.

Utilizing the adhesive strength of the CNT-to-CNT contact, we have demonstrated a programmable three-terminal micro-switching device. The low adhesion between the CNT arrays can suppress stiction failures even in repeatable hot-switching, and it also offers an opportunity for realizing memory logic in this microscale device. An external sensing resistor of 2 kΩ was

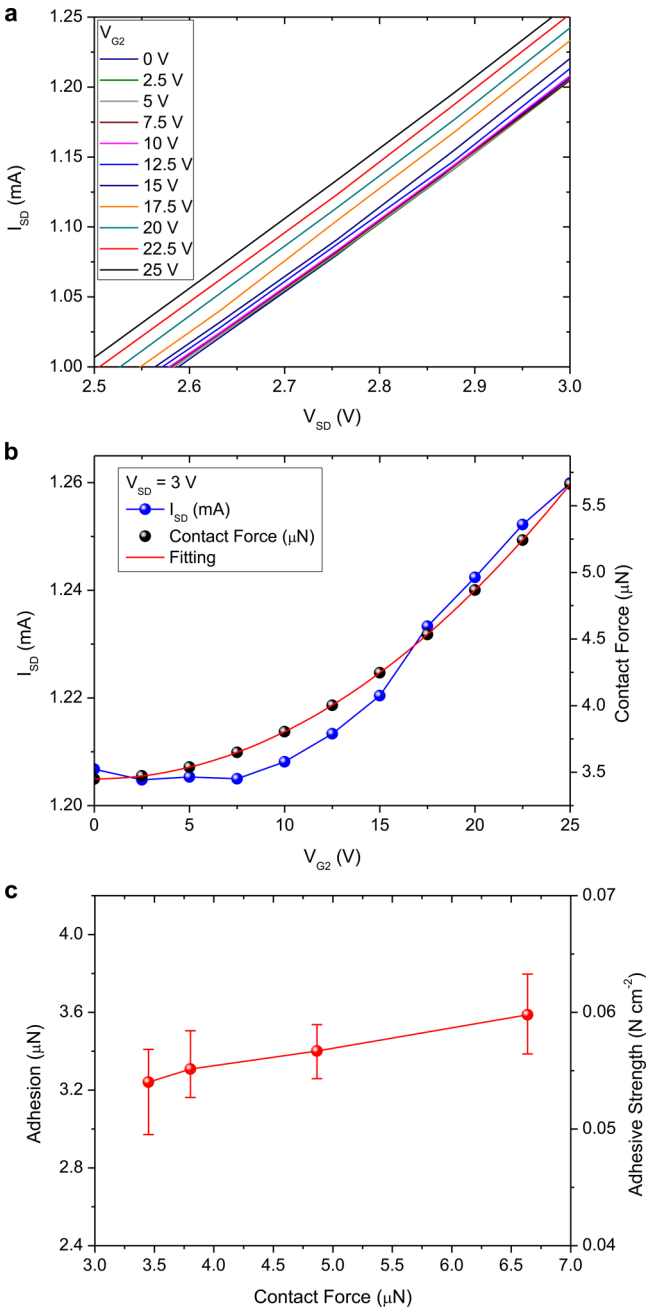

Figure 4. (a) The slope of the I_{SD}−V_{SD} curves increases as V_{G2} increases. (b) The larger contact force increases the number of CNTs in contact and decreases the contact resistance between CNTs (increased I_{SD} at constant V_{SD}). (c) The adhesion between CNT arrays increases as the contact force increases.

connected across the contact to record the voltage drop, while the applied V_{G1} was simultaneously monitored. The V_{G1} was programmed to write, read, and erase, whereas the V_{SD} was held constant at 1.5 V. Since the pull-out voltage was 43.5 V at V_{G2} of 0 V, the on-state remained at 42 V. However, after the contact was turned off at 50 V, this off-state was maintained until the initial pull-in at 40 V. Therefore, two different states of the contact existed at V_{G1} = 42 V according to preceding actuation of the shuttle. As shown in continuous (i) write, (ii) read ('1'), (iii) erase, and (iv) read ('0') cycles of Figure 5a, this mechanical contact could be configured as low- and high-resistance states with high on/off ratio. The dimension of

dx.doi.org/10.1021/am500252s | ACS Appl. Mater. Interfaces 2014, 6, 6598−6605

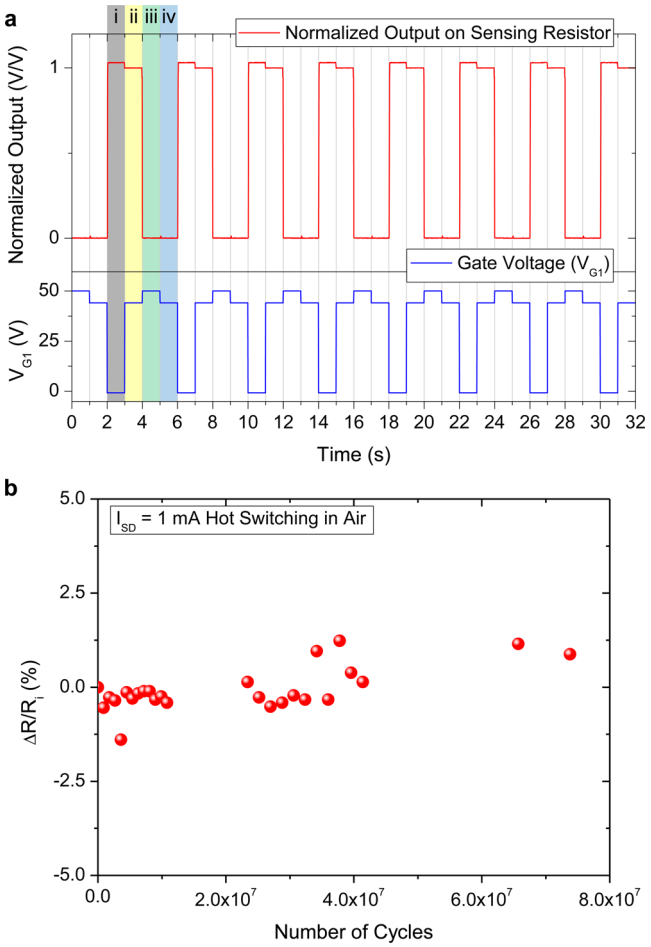

Figure 5. (a) The voltage V_{G1} is sequentially programmed to (i) 0, (ii) 42, (iii) 50, and (iv) 42 V. Because of the adhesion between the CNTs, the contact has two different states (low and high resistance) at V_{G1} = 42 V according to the preceding operation of the shuttle. (b) The contact is hot-switched for 7.3×10^7 cycles of 1 mA on/off operation, and relative resistance change in resistance is less than 1.4%, revealing high reliability and stability of the contact between CNTs.

switching device could be downscaled for reducing operation voltage, and further optimization and miniaturization should be conducted for more practical use of CNT-based contact.

Moreover, in terms of the reliability and durability, the CNT-to-CNT contact is preferred over typical solid contact materials such as gold. Because of its softness, gold-to-gold contacts generally require high release forces of $\sim 10^2 - 10^3$ μN,[43] and accordingly it suffers from in-use stiction failure. In addition, unavoidable surface degradations from wear, abrasion, welding, and melting also cause early failures in most solid contact materials. On the other hand, the low adhesion and wear resistance of CNTs may improve the reliability of the contact. We verified the reliability and durability experimentally by measuring the resistance between the source and drain electrodes for 7.3×10^7 cycles of 1 mA hot-switching on/off operation in an air environment. The relative resistance change of the contact was less than 1.4%, indicating both mechanical and electrical stability of the CNTs, as shown in Figure 5b, and the pull-out and pull-in voltages were also constant.

CONCLUSIONS

In conclusion, we investigated the adhesion between the top ends of aligned CNTs integrated on an electrostatically driven bidirectional actuator. While the actuator provided both contact force and pull-out force on the contact, the entire pull-out and pull-in behaviors were measured by the change in the electrical resistance between the CNTs. The estimated adhesion and contact geometries between the top ends of the CNTs agreed with the theoretical van der Waals force values, whereas the effects of the capillary forces and contact softening were negligible. We found that the adhesion between the top ends of the CNTs had a lower bound value than the adhesion between the sidewalls of the CNTs; however, this adhesion was sufficient for demonstrating a programmable microelectromechanical switch. The contact between the top ends of the CNTs could be extended for diverse applications, which require low adhesion but stable and reliable electromechanical contacts, in the fields of nanoelectromechanical systems and nanotribology.

EXPERIMENTAL SECTION

Fabrication of the Microelectromechanical Structures. Both sides of a 4-in Si-on-insulator wafer were thermally oxidized, patterned by photolithography, and etched by deep reactive ion etching. Then, the wafer was diced to chip scale (1×1 cm^2) by laser machining, and the remaining photoresist was completely stripped off. After release of any movable structures with hydrofluoric acid, the 5-nm-thick iron catalyst for CNT growth was deposited by electron-beam evaporation through a shadow mask.

Growth of the CNT Arrays. The chip was loaded in a single-zone tube furnace (Lindberg Blue M TF55030C). The tube was evacuated to 2 Torr and purged with 100 sccm of nitrogen. After the temperature of the furnace reached 700 °C, 100 sccm of ammonia was supplied for 30 min to pretreat the iron catalyst, and 30 sccm of acetylene was subsequently introduced for 15 min to initiate growth of the CNTs. The two sets of facing CNTs were self-adjusted during the growth, making contact with their top ends.[27]

Measurements and Characterizations of the Adhesion. A sourcemeter (Keithley 2400) and a digital multimeter (Agilent 34405A) were used for the application and measurement of V_{SD} and I_{SD}. To pull out the CNT arrays, the voltage was applied on V_{G1} through a direct-current (dc) power supply (Agilent E3647A). Alternatively, a function generator (Agilent 33220A) and a voltage amplifier (FLC Electronics F20AD) were used for repeated switching tests. Another dc power supply was used to apply the voltage on V_{G2} for tuning the contact force. To measure the response of the switch, the applied voltage on V_{G1} and a voltage drop across the sensing resistor were simultaneously recorded by an oscilloscope (Agilent DSO5014A). The dependency of the adhesion on the RH and temperature was measured both in a humidity-controlled environmental chamber (HANYOUNGNUX TH500) and in a forced convection oven (JEIO TECH OF-02GW). The contact between the CNTs was exposed in each level of the RH and temperature for more than 2 h before the measurements. All of the values in Figures 3b,c and 4c were an average of 25 measurements for each RH, temperature, and applied V_{G2}. The increment of V_{G1} to obtain the pull-out voltage was 0.1 V.

ASSOCIATED CONTENT

Supporting Information

Fabrication process of the microactuator and growth of the CNT arrays, measurements of the spring stiffness, contact force, and electrostatic force, force balance during pull-out, estimation of the number of CNTs in contact, comparison of the adhesion between individual CNTs, and hysteretic $I_{SD}-V_{G1}$ curves and adhesion between the CNT arrays with respect to

dx.doi.org/10.1021/am500252s | ACS Appl. Mater. Interfaces 2014, 6, 6598−6605

the applied V_{G2}. This material is available free of charge via the Internet at http://pubs.acs.org.

AUTHOR INFORMATION

Corresponding Author

*E-mail: kimjb@yonsei.ac.kr.

Notes

The authors declare no competing financial interest.

ACKNOWLEDGMENTS

This research was supported by the Center for Integrated Smart Sensors as a Global Frontier Project (CISS-2012M3A6A6054201) and by the Fusion Research Program for Green Technologies (Grant NRF-2010-0019088) through the National Research Foundation of Korea (NRF) funded by the Ministry of Science, ICT and Future Planning, and by the NRF Grant funded by the Korean Government (Ministry of Education; Grant NRF-2012R1A1A2043661).

REFERENCES

(1) Jeong, H. E.; Suh, K. Y. Nanohairs and Nanotubes: Efficient Structural Elements for Gecko-Inspired Artificial Dry Adhesives. *Nano Today* **2009**, *4*, 335−346.

(2) Boesel, L. F.; Greiner, C.; Arzt, E.; del Campo, A. Gecko-Inspired Surfaces: A Path to Strong and Reversible Dry Adhesives. *Adv. Mater.* **2010**, *22*, 2125−2137.

(3) Yurdumakan, B.; Raravikar, N. R.; Ajayan, P. M.; Dhinojwala, A. Synthetic Gecko Foot-Hairs from Multiwalled Carbon Nanotubes. *Chem. Commun.* **2005**, 3799−3801.

(4) Zhao, Y.; Tong, T.; Delzeit, L.; Kashani, A.; Meyyappan, M.; Majumdar, A. Interfacial Energy and Strength of Multiwalled-Carbon-Nanotube-Based Dry Adhesive. *J. Vac. Sci. Technol. B* **2006**, *24*, 331−335.

(5) Qu, L.; Dai, L. Gecko-Foot-Mimetic Aligned Single-Walled Carbon Nanotube Dry Adhesives with Unique Electrical and Thermal Properties. *Adv. Mater.* **2007**, *19*, 3844−3849.

(6) Ge, L.; Sethi, S.; Ci, L.; Ajayan, P. M.; Dhinojwala, A. Carbon Nanotube-Based Synthetic Gecko Tapes. *Proc. Natl. Acad. Sci. U. S. A.* **2007**, *104*, 10792−10795.

(7) Sethi, S.; Ge, L.; Ci, L.; Ajayan, P. M.; Dhinojwala, A. Gecko-Inspired Carbon Nanotube-Based Self-Cleaning Adhesives. *Nano Lett.* **2008**, *8*, 822−825.

(8) Qu, L.; Dai, L.; Stone, M.; Xia, Z.; Wang, Z. L. Carbon Nanotube Arrays with Strong Shear Binding-On and Easy Normal Lifting-Off. *Science* **2008**, *322*, 238−242.

(9) Maeno, Y.; Nakayama, Y. Geckolike High Shear Strength by Carbon Nanotube Fiber Adhesives. *Appl. Phys. Lett.* **2009**, *94*, 012103.

(10) Yu, M. F.; Kowalewski, T.; Ruoff, R. S. Structural Analysis of Collapsed, and Twisted and Collapsed, Multiwalled Carbon Nanotubes by Atomic Force Microscopy. *Phys. Rev. Lett.* **2001**, *86*, 87−90.

(11) Johnson, K. L.; Kendall, K.; Roberts, A. D. Surface Energy and the Contact of Elastic Solids. *Proc. R. Soc. London, A* **1971**, *324*, 301−313.

(12) Poggi, M. A.; Bottomley, L. A.; Lillehei, P. T. Measuring the Adhesion Forces between Alkanethiol-Modified AFM Cantilevers and Single Walled Carbon Nanotubes. *Nano Lett.* **2004**, *4*, 61−64.

(13) Whittaker, J. D.; Minot, E. D.; Tanenbaum, D. M.; McEuen, P. L.; Davis, R. C. Measurement of the Adhesion Force between Carbon Nanotubes and a Silicon Dioxide Substrate. *Nano Lett.* **2006**, *6*, 953−957.

(14) Chen, B.; Gao, M.; Zuo, J. M.; Qu, S.; Liu, B.; Huang, Y. Binding Energy of Parallel Carbon Nanotubes. *Appl. Phys. Lett.* **2003**, *83*, 3570−3571.

(15) Bhushan, B.; Ling, X.; Jungen, A.; Hierold, C. Adhesion and Friction of a Multiwalled Carbon Nanotube Sliding Against Single-Walled Carbon Nanotube. *Phys. Rev. B* **2008**, *77*, 165428.

(16) Bhushan, B.; Ling, X. Adhesion and Friction between Individual Carbon Nanotubes Measured Using Force-Versus-Distance Curves in Atomic Force Microscopy. *Phys. Rev. B* **2008**, *78*, 045429.

(17) Ke, C.; Zheng, M.; Zhou, G.; Cui, W.; Pugno, N.; Miles, R. N. Mechanical Peeling of Free-Standing Single-Walled Carbon-Nanotube Bundles. *Small* **2010**, *6*, 438−445.

(18) Kim, P.; Lieber, C. M. Nanotube Nanotweezers. *Science* **1999**, *286*, 2148−2150.

(19) Rueckes, T.; Kim, K.; Joselevich, E.; Tseng, G. Y.; Cheung, C. L.; Lieber, C. M. Carbon Nanotube-Based Nonvolatile Random Access Memory for Molecular Computing. *Science* **2000**, *289*, 94−97.

(20) Jang, J. E.; Cha, S. N.; Choi, Y.; Amaratunga, G. A. J.; Kang, D. J.; Hasko, D. G.; Jung, J. E.; Kim, J. M. Nanoelectromechanical Switches with Vertically Aligned Carbon Nanotubes. *Appl. Phys. Lett.* **2005**, *87*, 163114.

(21) Hayamizu, Y.; Yamada, T.; Mizuno, K.; Davis, R. C.; Futaba, D. N.; Yumura, M.; Hata, K. Integrated Three-Dimensional Microelectromechanical Devices from Processable Carbon Nanotube Wafers. *Nat. Nanotechnol.* **2008**, *3*, 289−294.

(22) Choi, J.; Lee, J. I.; Eun, Y.; Kim, M. O.; Kim, J. Aligned Carbon Nanotube Arrays for Degradation-Resistant, Intimate Contact in Micromechanical Devices. *Adv. Mater.* **2011**, *23*, 2231−2236.

(23) Lee, J. I.; Song, Y.; Jung, H.; Choi, J.; Eun, Y.; Kim, J. Deformable Carbon Nanotube-Contact Pads for Inertial Microswitch to Extend Contact Time. *IEEE Trans. Ind. Electron.* **2012**, *59*, 4914−4920.

(24) Eun, Y.; Lee, J. I.; Choi, J.; Song, Y.; Kim, J. Integrated Carbon Nanotube Array as Dry Adhesive for High-Temperature Silicon Processing. *Adv. Mater.* **2011**, *23*, 4285−4289.

(25) Cao, A.; Veedu, V. P.; Li, X.; Yao, Z.; Ghasemi-Nejhad, M. N.; Ajayan, P. M. Multifunctional Brushes Made from Carbon Nanotubes. *Nat. Mater.* **2005**, *4*, 540−545.

(26) Toth, G.; Mäklin, J.; Halonen, N.; Palosaari, J.; Juuti, J.; Jantunen, H.; Kordas, K.; Sawyer, W. G.; Vajtai, R.; Ajayan, P. M. Carbon-Nanotube-Based Electrical Brush Contacts. *Adv. Mater.* **2009**, *21*, 2054−2058.

(27) Choi, J.; Pyo, S.; Baek, D. H.; Lee, J. I.; Kim, J. Thickness-, Alignment- and Defect-Tunable Growth of Carbon Nanotube Arrays Using Designed Mechanical Loads. *Carbon* **2014**, *66*, 126−133.

(28) Cola, B. A.; Xu, J.; Fisher, T. S. Contact Mechanics and Thermal Conductance of Carbon Nanotube Array Interfaces. *Int. J. Heat Mass Transfer* **2009**, *52*, 3490−3503.

(29) Hart, A. J.; Slocum, A. H. Force Output, Control of Film Structure, and Microscale Shape Transfer by Carbon Nanotube Growth under Mechanical Pressure. *Nano Lett.* **2006**, *6*, 1254−1260.

(30) Ng, K. K.; Liu, R. On the Calculation of Specific Contact Resistivity on ⟨100⟩ Si. *IEEE Trans. Electron Devices* **1990**, *37*, 1535−1537.

(31) Choi, J.; Kim, J. Batch-Processed Carbon Nanotube Wall as Pressure and Flow Sensor. *Nanotechnology* **2010**, *21*, 105502.

(32) Yang, D. J.; Wang, S. G.; Zhang, Q.; Sellin, P. J.; Chen, G. Thermal and Electrical Transport in Multi-Walled Carbon Nanotubes. *Phys. Lett. A* **2004**, *329*, 207−213.

(33) Nirmalraj, P. N.; Lyons, P. E.; De, S.; Coleman, J. N.; Boland, J. J. Electrical Connectivity in Single-Walled Carbon Nanotube Networks. *Nano Lett.* **2009**, *9*, 3890−3895.

(34) Bedewy, M.; Meshot, E. R.; Reinker, M. J.; Hart, A. J. Population Growth Dynamics of Carbon Nanotubes. *ACS Nano* **2011**, *5*, 8974−8989.

(35) Bhushan, B. Adhesion and Stiction: Mechanisms, Measurement Techniques, and Methods for Reduction. *J. Vac. Sci. Technol. B* **2003**, *21*, 2262−2296.

(36) Li, H.; Wang, X.; Song, Y.; Liu, Y.; Li, Q.; Jiang, L.; Zhu, D. Super-"Amphiphobic" Aligned Carbon Nanotube Films. *Angew. Chem., Int. Ed.* **2001**, *40*, 1743−1746.

(37) Fraden, J. *Handbook of Modern Sensors*, 4th ed.; Springer: Berlin, 2010.

(38) Israelachvili, J. N. *Intermolecular and Surface Forces*, 3rd ed.; Academic Press: New York, 2011.

(39) Dong, L.; Arai, F.; Fukuda, T. Nanoassembly of Carbon Nanotubes through Mechanochemical Nanorobotic Manipulations. *Jpn. J. Appl. Phys.* **2003**, *42*, 295−298.
(40) Li, Y.; Hu, N.; Yamamoto, G.; Wang, Z.; Hashida, T.; Asanuma, H.; Dong, C.; Okabe, T.; Arai, M.; Fukunaga, H. Molecular Mechanics Simulation of the Sliding Behavior between Nested Walls in a Multi-Walled Carbon Nanotube. *Carbon* **2010**, *48*, 2934−2940.
(41) Yamamoto, G.; Liu, S.; Hu, N.; Hashida, T.; Liu, Y.; Yan, C.; Li, Y.; Cui, H.; Ning, H.; Wu, L. Prediction of Pull-Out Force of Multi-Walled Carbon Nanotube (MWCNT) in Sword-in-Sheath Mode. *Comput. Mater. Sci.* **2012**, *60*, 7−12.
(42) Wang, T.; Jeppson, K.; Ye, L.; Liu, J. Carbon-Nanotube Through-Silicon Via Interconnects for Three-Dimensional Integration. *Small* **2011**, *7*, 2313−2317.
(43) Oberhammer, J.; Stemme, G. Active Opening Force and Passive Contact Force Electrostatic Switches for Soft Metal Contact Materials. *J. Microelectromech. Syst.* **2006**, *15*, 1235−1242.